Turkish Journal of Electrical Engineering & Computer Sciences

http://journals.tubitak.gov.tr/elektrik/

Research Article

Turk J Elec Eng & Comp Sci
(2022) 30: 695 – 712

doi:10.3906/elk-2105-142

Determining allowable parametric uncertainty in an uncommon quadrotor model for closed loop stability

Mehmet BASKIN[1,*], **Kemal LEBLEBİCİOĞLU**[2]
[1]Aselsan Inc., Ankara, Turkey
[2]Department of Electrical-Electronics Engineering, Middle East Technical University, Ankara, Turkey

Received: 16.05.2021 • **Accepted/Published Online:** 25.12.2021 • **Final Version:** 21.03.2022

Abstract: In this article, control oriented uncertainty modeling of an uncommon quadrotor in hover is discussed. This quadrotor consists of two counter-rotating big rotors on longitudinal axis and two counter-rotating small tilt rotors on lateral axis. Firstly, approximate linear model of this vehicle around hover is obtained by using Newton–Euler formulation. Secondly, specific uncertainty is assigned to each parameter. Resulting uncertain model is converted into a linear fractional transformation framework for robustness analysis. Next, the most critical uncertain parameters in terms of robust stability in a proposed quadrotor model are investigated using μ sensitivities. Finally, skewed-μ analysis determines maximum possible uncertainty bounds for model parameters that are difficult to identify accurately.

Key words: Parameter uncertainty, sensitivity analysis, quadrotor, structured singular value, unmanned aerial vehicle

1. Introduction

The popularity of unmanned aerial vehicles (UAVs) has greatly increased in academic research and commercial areas. Recently, quadrotors have become the most common configuration owing to vertical take off and landing (VTOL), hovering, and maneuverability capabilities. These vehicles have become popular in many military and civil applications with the help of low-cost hardware and simple structure [1, 2]. However, quadrotors suffer from high energy consumption, and they typically have less than 20-min flight endurance due to inadequate stored energy per unit mass of available batteries [3, 4]. Therefore, using alternative power source and improving efficiency of lifting system have been investigated recently [4, 6–9].

Required power to maintain thrust over a rotor disc changes exponentially with total weight and inverse of the rotor disc area [4, 5]. It is known that total rotor area in the unit footprint is smaller for quadrotors than helicopters. On the other hand, helicopters have mechanically complex and fragile rotor systems, which require intensive maintenance. For that reason, researchers have tried to combine simple and robust quadrotor structure and efficiency of helicopters.

The triangular quadrotor consists of large rotor in the center to provide lift and canted three small rotors for control, and counter torque is introduced in [4]. While improving efficiency by 15 percent, this configuration has degraded hover attitude control performance due to uncompensated gyroscopic torque of the main rotor.

Using hydrocarbon fuel as an alternative power source significantly outperforms the battery powered propulsion system, and it gives relatively large flight endurance. In [6], coaxial inverting thruster using two

*Correspondence: mbaskin@aselsan.com.tr

gasoline engines is placed at the center of a standard quadrotor. In this configuration, gyroscopic and counter torques are compensated, but efficiencies of coaxial rotors decrease. Next, a new configuration based on variable pitch rotors that are powered by a gasoline engine is introduced in [7]. This configuration requires very complex drivetrain and four variable pitch rotors. Therefore, this configuration is more fragile, and it is rather prone to failure. Flight duration is significantly improved for these cases. Moreover, two new configurations based on four-gasoline engine and four-combined electrical motor-gasoline engine are proposed in [8] and [9], respectively. These vehicles are specifically proposed to lift very large weights with a dramatic rise in their cost due to required four gasoline engines.

From control theory point of view, different control techniques have been introduced in the past years. Nested control loops for position and attitude was proved to be successful for standard quadrotors in different projects. PD type attitude controller and PID type position controller have become the most popular selection [5]. However, these controllers guarantee stability when the vehicle is around hover position, and parameters are known accurately. Next, to stabilize the system under parameter variations or to increase the operating range further from hover position, nonlinear $\mathcal{H}_\infty$ control [10], intelligent controller [11], and robust adaptive controller [12] are used. In these studies, mainly parametric uncertainties in the mass and inertia terms are considered.

1.1. Summary of contributions

Key contributions made in this article can be summarized as following:

- An uncommon quadrotor configuration is proposed to increase the efficiency and, hence, flight endurance compared to a standard quadrotor.

- Structured singular value (μ) sensitivity and skewed-μ analyses are used for the first time for a multirotor to analyze the effects of uncertain parameters and to determine their maximum allowable deviations in terms of closed loop stability.

1.1.1. An uncommon quadrotor configuration

In this article, an uncommon quadrotor configuration is proposed. It aims to solve the uncompensated gyroscopic torque problem for a single large rotor and low efficiency problem for coaxial large rotors. In this case, two counter-rotating large rotors are placed on the longitudinal axis to minimize the effects of gyroscopic and rotor drag torques. On lateral axis, small counter-rotating rotors are used for attitude control. In addition, distance between small rotor and body is kept small to avoid large vehicle horizontal width. Weight of the vehicle is mostly carried by large rotors in this design. Therefore, a more efficient configuration can be obtained according to momentum theory, since carrying the same weight with two large rotor is more efficient than other multirotor configurations for the same vehicle horizontal width [13]. Unlike a standard quadrotor, alternate rotors are not counter-rotating to minimize rotor drag and gyroscopic torques. Herein, small rotors need tilt ability to control yaw motion. This configuration may resemble the Boeing CH-47 Chinook, but two tiltable small rotors replace a complex swashplate mechanism for attitude control. Moreover, replacing large electrical motors with gasoline engines significantly improves the payload capacity and flight endurance with lower cost than the four-gasoline engine configuration discussed in [8, 9]. In short, this uncommon configuration is planned to combine the mechanical simplicity of a quadrotor and efficiency of a tandem rotor helicopter.

1.1.2. μ sensitivity and skewed-μ analyses

Mathematical model, which is accompanied by an uncertainty model, is generally used for control design purpose. If system identification methods are preferred, suitable control relevant nominal model with suitable uncertainty representation is needed [14, 15]. If these methods are not used, model based on physical principles is selected. In this case, bounds on model parameters are used as reported in [16], and a controller, which gives sufficient performance under these parameter variations, is aimed. But required robustness may not be achieved if variations in these parameters are large. In that case, uncertainty in some parameters should be reduced. Therefore, important parameters for robust stability or performance should be determined.

Traditionally, open loop eigenvalue sensitivity analysis is used. However, important parameters for open loop may be completely different from closed loop after a controller is designed. Moreover, closed loop eigenvalue sensitivity analysis may also provide inadequate information. Closed loop μ sensitivity analysis is useful to determine the parameters that limit the closed loop stability. In addition, some of the parameters in the model are much more difficult to estimate. Therefore, this analysis also determines the maximum allowable uncertainty in these parameters without violating closed loop stability. This is mostly valuable in aerospace control applications where there are large uncertainty in the parameters, and identification tests are difficult and expensive. In literature, different techniques can be found for control of multirotors under parametric uncertainties [10–12]. However, to the author's knowledge, previous works do not investigate the relative importance of different uncertain parameters for closed loop stability. In addition, how allowable uncertainties of some parameters change when remaining parameters are known more accurately is not analyzed. In this article, μ sensitivities and skewed-μ analysis are used for these purposes.

1.2. Organization of the article

In Section 2, nonlinear dynamic model of the proposed quadrotor configuration is obtained by using Newton–Euler formulation. Herein, aerodynamic effects such as thrust change due to large angle of attack and high speed, blade flapping, and interference effects are neglected, and only principal dynamics are used during modeling [5]. Since this vehicle is planned to be used at slow velocities around hover, this assumption is reasonable, and these effects can be considered as disturbance sources. In Section 3, approximate linear model around hover is obtained. Herein, resulting model is very similar to a usual quadrotor, with the exception of the rotor mixing (decoupling) matrix. In Section 4, uncertain model is constructed by assigning an uncertainty to each parameter. Next, which uncertain parameters in a proposed quadrotor model are most critical in terms of robust stability is investigated using μ sensitivities. Finally, skewed-μ analysis determines maximum possible uncertainty bounds for model parameters that are difficult to identify accurately.

2. Dynamical model

Similar to a common quadrotor, the proposed configuration consists of five rigid bodies, namely quadrotor body B and four rotor groups P_i. Big rotors $(i = 1, 3)$ are placed on the longitudinal axis, and small tilt rotors $(i = 2, 4)$ are placed on the lateral axis. In this section, motion equations of this system are derived.

2.1. Preliminary definitions

Let $\mathcal{F}_E : \{O_E; x_E, y_E, z_E\}$ be an earth inertial frame and $\mathcal{F}_B : \{O_B; x_B, y_B, z_B\}$ be a quadrotor body frame attached to its mass center. In addition, fixed rotor frames $\mathcal{F}_{P_i} : \{O_{P_i}; x_{P_i}, y_{P_i}, z_{P_i}\}$, $i = 1, 2, 3, 4$ are taken as

parallel to each other and body frame. Second and forth rotors change their orientation by rotating around y_{P_i} by an angle of α_i. This rotation creates a new rotating frame for small rotors as shown in Figure 1, and they are denoted by $\mathcal{F}_{\bar{P}_i} : \{O_{\bar{P}_i}; x_{\bar{P}_i}, y_{\bar{P}_i}, z_{\bar{P}_i}\},\ i = 2, 4$.

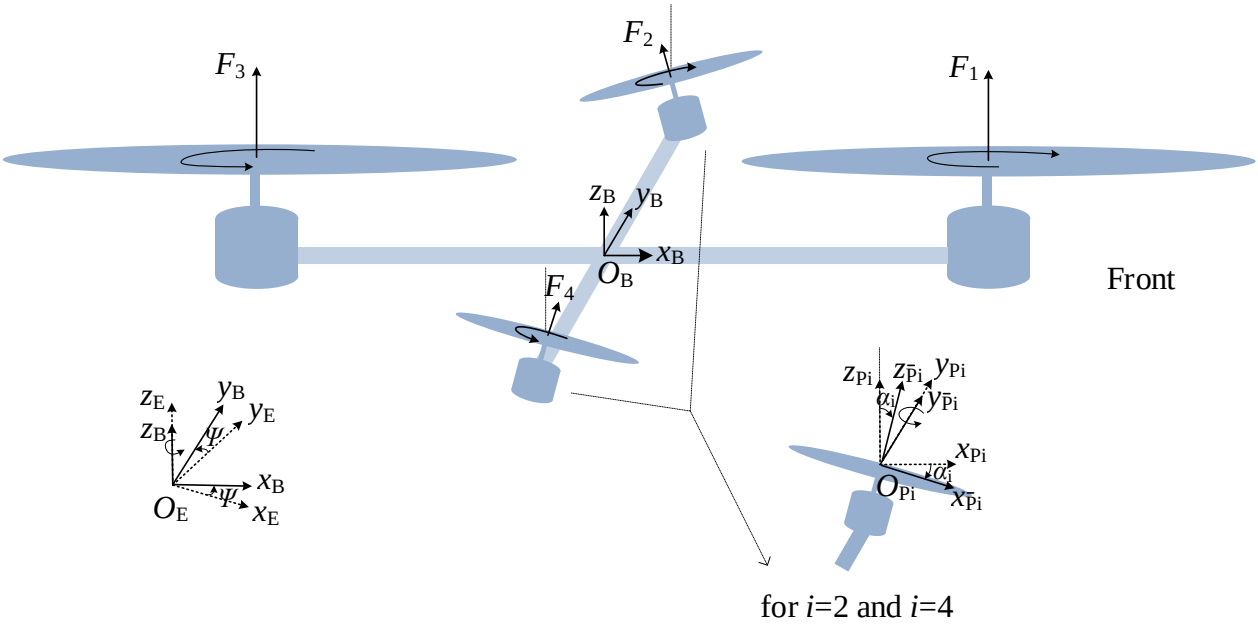

Figure 1. An uncommon quadrotor configuration.

In this configuration, similar type motors must rotate in opposite directions to cancel out gyroscopic and counter torques in hover. Herein, rotor 1 and 2 rotate in clockwise (CW) direction, and rotor 3 and 4 rotate in counter clockwise (CCW) direction.

Translational coordinates in the inertial frame is represented by the vector $\xi = [x\ y\ z]^T$, and three Euler angles $\eta = [\phi\ \theta\ \psi]^T$ denote the orientation of the vehicle. Roll angle ϕ, pitch angle θ, and yaw angle ψ correspond to the rotation around the x, y and z-axis, respectively. Then, resulting rotation matrix from body frame to inertial frame can be obtained from three successive rotations as $R_B^E = R_Z(\psi)R_Y(\theta)R_X(\phi)$ that is given by (1) where $sx = \sin(x)$ and $cx = \cos(x)$.

$$R_B^E = \begin{bmatrix} c\psi c\theta & -s\psi c\phi + c\psi s\theta s\phi & s\psi s\phi + c\psi s\theta c\phi \\ s\psi c\theta & c\psi c\phi + s\psi s\theta s\phi & -c\psi s\phi + s\psi s\theta c\phi \\ -s\theta & c\theta s\phi & c\theta c\phi \end{bmatrix} \tag{1}$$

In addition, let $R_{\bar{P}_i}^{P_i}$ be the rotation matrix from rotating rotor frame $\mathcal{F}_{\bar{P}_i}$ to rotor-fixed frame $\mathcal{F}_{P_i}$ for $i = 2, 4$ where α_i is the tilt angle of the $i-$th rotor. This rotation matrix given in (2) also equals to $R_{\bar{P}_i}^B$, since $\mathcal{F}_B$ and $\mathcal{F}_{\bar{P}_i}$ are parallel.

$$R_{\bar{P}_i}^{P_i} = R_{\bar{P}_i}^B = \begin{bmatrix} c\alpha_i & 0 & s\alpha_i \\ 0 & 1 & 0 \\ -s\alpha_i & 0 & c\alpha_i \end{bmatrix} \tag{2}$$

Rates of Euler angles $[\dot{\phi}\ \dot{\theta}\ \dot{\psi}]^T$ can be obtained from body frame angular rates $[p\ q\ r]^T$ as (3) where

$tx = \tan(x)$.

$$\begin{bmatrix} \dot{\phi} \\ \dot{\theta} \\ \dot{\psi} \end{bmatrix} = \begin{bmatrix} 1 & s\phi t\theta & c\phi t\theta \\ 0 & c\phi & -s\phi \\ 0 & s\phi/c\theta & c\phi/c\theta \end{bmatrix} \begin{bmatrix} p \\ q \\ r \end{bmatrix} \tag{3}$$

2.2. Equations of motion

The motion equations of a rigid body are derived by using Newton–Euler formulation as follows:

$$m\dot{V}^B + \Omega \times mV^B = F^B \ , \tag{4}$$

$$I\dot{\Omega} + \Omega \times I\Omega = \Gamma^B \ , \tag{5}$$

where F^B and Γ^B are the total force and torque applied to center of gravity, and m is the mass of a vehicle. Herein, $\Omega = [p \ q \ r]^T$ denotes the body frame angular rate, and $V^B = [\dot{x}^B \ \dot{y}^B \ \dot{z}^B]^T$ denotes the translational velocity. In addition, I corresponds to the moments of inertia about body-fixed frame $\mathcal{F}_B$.

2.2.1. Translational motion

Tilt rotors provide thrust components affecting both translational and rotational motion as $F_i^B = R_{\bar{P}_i}^B F_i^{\bar{P}_i}$, $i = 2, 4$. Similarly, fixed rotors provide thrust as $F_i^B = F_i^{\bar{P}_i}$, $i = 1, 3$. Thrust generated by the corresponding rotor is modeled as $F_i^{\bar{P}} = [0 \ 0 \ k_{f_i} w_i^2]^T$ where k_{f_i} and w_i denote the thrust constant and rotating speed of the $i-$th rotor, respectively [1]. In the inertial frame, translational motion of a vehicle can be derived from

$$m\dot{V}^E = mG^E + R_B^E T^B \ , \tag{6}$$

where $G^E = [0 \ 0 \ -g]^T$ is the gravity vector, $T^B = \left(\sum_{i=1}^4 F_i^B\right)$ is the total thrust vector, and $V^E = \dot{\xi}$.

2.2.2. Rotational motion

The Γ^B term in (5) includes three main torque components.

1. Actuators torque: Actuators torque can be obtained by $\Gamma_A^B = \left(\sum_{i=1}^4 l_i^B \times F_i^B\right)$ where $l_1^B = [l_b \ 0 \ l_{bh}]^T$, $l_2^B = [0 \ l_s \ l_{sh}]^T$, $l_3^B = [-l_b \ 0 \ l_{bh}]^T$, $l_4^B = [0 \ -l_s \ l_{sh}]^T$ are distances from the mass center to rotors where l_b and l_s denote the big and small arm length of the quadrotor, respectively. In addition, l_{bh} and l_{sh} denote the distance from the mass center to big and small rotor along z-axis, respectively.

2. Gyroscopic torque: Gyroscopic torque due to rotors is given by $\Gamma_G^B = \left(\sum_{i=1}^4 I_{R_i}(\Omega \times \bar{W}_i^B)\right)$ where $\bar{W}_i^B$ and I_{R_i} correspond to velocity vector in body frame and inertia of the $i-$th rotor, respectively.

3. Rotor drag torque: Rotor drag torque about the mass center of the vehicle is taken as $\Gamma_D^B = \left(\sum_{i=1}^4 R_{\bar{P}_i}^B D_i^{\bar{P}_i}\right)$ where $D_i^{\bar{P}} = [0 \ 0 \ -\sigma_i k_{d_i} w_i^2]^T$ is the counter-rotating torque generated about the $z_{\bar{P}_i}$ axis where k_{d_i} denotes the drag torque constant of the $i-$th rotor [1]. Here, $\sigma_i \in \{-1, 1\}$ denotes direction of rotor. For positive rotation around $z_{\bar{P}_i}$ axis σ_i=1 is used, whereas negative rotation requires σ_i=-1.

It is accepted that quadrotor is symmetric, and its inertia matrix is $I = \text{diag}(I_{xx}, I_{yy}, I_{zz})$. Overall motion equations (7) and (8) of an uncommon quadrotor are obtained from (5) and (6) where $\Gamma^B = \Gamma_A^B + \Gamma_D^B - \Gamma_G^B$.

In addition, rate of the Euler angles is obtained from (3) by using body frame rates.

$$\ddot{\xi} = G^E + \frac{1}{m} R_B^E T^B \tag{7}$$

$$\dot{\Omega} = I^{-1}(-\Omega \times I\Omega + \Gamma^B) \tag{8}$$

3. Motion control for the proposed quadrotor

Full nonlinear model in (7) and (8) is suitable for simulation of the vehicle motion. For control design and robustness analysis purposes, simple model is desirable, since the rotational motion equations are fairly complex. It is assumed that bandwidth of rotor speed control is high, and transients on motor speeds are neglected. In this way, w_i's are considered as control inputs instead of motor torques. Simpler model is obtained by neglecting second order inertial and gyroscopic terms. In slow flight conditions, these terms are rather smaller than the forces and torques generated by propellers. Therefore, these terms are considered as disturbance sources which are minimized by the attitude control loop. Therefore, simplified rotational motion equation, $\dot{\Omega} = I^{-1}\Gamma^B$ is used for controller design and robustness analysis goals where Γ^B is simplified as $\Gamma^B = \Gamma_A^B + \Gamma_D^B$.

Finally, translational and simplified rotational motion equations are given in a compact form as (9) and (10) where $w = [w_1^2 \; w_2^2 \; w_3^2 \; w_4^2]^T$ denotes the manipulated variables, and $F(\alpha)$ and $\tau(\alpha)$ are given in (11).

$$\ddot{\xi} = G^E + \frac{1}{m} R_B^E F(\alpha) w \tag{9}$$

$$\dot{\Omega} = I^{-1}\tau(\alpha) w \tag{10}$$

$$F(\alpha) = \begin{bmatrix} 0 & k_{f_s} s\alpha_2 & 0 & k_{f_s} s\alpha_4 \\ 0 & 0 & 0 & 0 \\ k_{f_b} & k_{f_s} c\alpha_2 & k_{f_b} & k_{f_s} c\alpha_4 \end{bmatrix}, \; \tau(\alpha) = \begin{bmatrix} 0 & k_{d_s} s\alpha_2 + k_{f_s} l_s c\alpha_2 & 0 & -k_{d_s} s\alpha_4 - k_{f_s} l_s c\alpha_4 \\ -k_{f_b} l_b & k_{f_s} l_{sh} s\alpha_2 & k_{f_b} l_b & k_{f_s} l_{sh} s\alpha_4 \\ k_{d_b} & k_{d_s} c\alpha_2 - k_{f_s} l_s s\alpha_2 & -k_{d_b} & -k_{d_s} c\alpha_4 + k_{f_s} l_s s\alpha_4 \end{bmatrix} \tag{11}$$

3.1. Linearization of the model in hover

The relation between body rates and rates of Euler angles (3), dynamic equations (9) and (10), manipulated variables $u = [w^T \; \alpha^T]^T$ where $\alpha = [\alpha_2 \; \alpha_4]^T$ and states $x = [(V^E)^T \; \eta^T \; \Omega^T]^T$ are used to obtain linearized model of the quadrotor in hover conditions. It includes only first-order terms in the Taylor series expansion of the nonlinear model around x_{eq} and u_{eq} [17].

3.1.1. Translational motion

The local linearization is obtained by expanding (9) around x_{eq} and u_{eq} where $\delta\eta$ and δu denote the perturbation from η_{eq} and u_{eq}.

$$\delta\ddot{\xi} = \frac{1}{m}\frac{\partial}{\partial\eta}\left(R_B^E F(\alpha) w\right)\Big|_{x_{eq},u_{eq}} \delta\eta + \frac{1}{m} R_B^E \frac{\partial}{\partial u}\left(F(\alpha) w\right)\Big|_{x_{eq},u_{eq}} \delta u \tag{12}$$

Let $\tilde{f} = F(\alpha)w$ and $(R_B^E)_i$ be the i^{th} column of the matrix and $\tilde{f}_i$ be the i^{th} entry of the vector. Then, following matrices are obtained from (12).

$$A_{trans} = \frac{1}{m}\sum_{i=1}^{3} \frac{\partial (R_B^E)_i}{\partial\eta} \tilde{f}_i \Big|_{x_{eq},u_{eq}}, \quad B_{trans} = \frac{1}{m} R_B^E \left[F(\alpha) \quad \sum_{i=1}^{4} \frac{\partial (F(\alpha))_i}{\partial\alpha} w_i \right] \Big|_{x_{eq},u_{eq}} \tag{13}$$

3.1.2. Rotational motion

Similarly, following results are obtained for rotational motion.

$$\dot{\Omega} = I^{-1}\frac{\partial}{\partial u}\left(\tau(\alpha)w\right)\Big|_{x_{eq},u_{eq}} \delta u \quad \rightarrow \quad B_{rot} = I^{-1}\left[\tau(\alpha) \quad \sum_{i=1}^{4}\frac{\partial(\tau(\alpha))_i}{\partial\alpha}w_i\right]\Big|_{x_{eq},u_{eq}} \tag{14}$$

3.1.3. Overall linearized model

The linearization is obtained around hover where $u = [w^T\ \alpha^T]^T = [w_{eq}^T\ 0\ 0]^T$ and states $x = [(V^E)^T\ \eta^T\ \Omega^T]^T = [0\ 0\ 0\ 0\ 0\ \psi\ 0\ 0\ 0]^T$. Herein, $w_{eq} = [w_{eq1}\ w_{eq2}\ w_{eq3}\ w_{eq4}]^T$ includes square of the hover rotor speeds. Around hover, $\dot{\eta} = \Omega$ is also satisfied for resulting linearized system. Finally, the overall linearized model (15) is obtained.

$$\begin{bmatrix}\delta\dot{V}^E\\ \delta\dot{\eta}\\ \delta\dot{\Omega}\end{bmatrix} = \begin{bmatrix}0 & A_{trans} & 0\\ 0 & 0 & I\\ 0 & 0 & 0\end{bmatrix}\begin{bmatrix}\delta V^E\\ \delta\eta\\ \delta\Omega\end{bmatrix} + \begin{bmatrix}B_{trans}\\ 0\\ B_{rot}\end{bmatrix}\begin{bmatrix}\delta w\\ \delta\alpha_2\\ \delta\alpha_4\end{bmatrix} \tag{15}$$

The submatrices in (15) are given below where $T = (k_{f_b}w_1^2 + k_{f_s}w_2^2 + k_{f_b}w_3^2 + k_{f_s}w_4^2)$ is the total thrust component in z-axis at hover conditions.

$$A_{trans} = \frac{1}{m}\begin{bmatrix}s\psi\ T & c\psi\ T & 0\\ -c\psi\ T & s\psi\ T & 0\\ 0 & 0 & 0\end{bmatrix} \quad , \quad B_{trans} = \frac{1}{m}\begin{bmatrix}0 & 0 & 0 & 0 & k_{f_s}w_{eq2}c\psi & k_{f_s}w_{eq4}c\psi\\ 0 & 0 & 0 & 0 & k_{f_s}w_{eq2}s\psi & k_{f_s}w_{eq4}s\psi\\ k_{f_b} & k_{f_s} & k_{f_b} & k_{f_s} & 0 & 0\end{bmatrix} \tag{16}$$

$$B_{rot} = I^{-1}\begin{bmatrix}0 & k_{f_s}l_s & 0 & -k_{f_s}l_s & k_{d_s}w_{eq2} & -k_{d_s}w_{eq4}\\ -k_{f_b}l_b & 0 & k_{f_b}l_b & 0 & k_{f_s}l_{sh}w_{eq2} & k_{f_s}l_{sh}w_{eq4}\\ k_{d_b} & k_{d_s} & -k_{d_b} & -k_{d_s} & -k_{f_s}l_sw_{eq2} & k_{f_s}l_sw_{eq4}\end{bmatrix}$$

4. Allowable parametric uncertainty in closed loop for the uncommon quadrotor model

In this section, which uncertain parameters in the proposed quadrotor model are most critical in terms of robust stability is investigated using μ sensitivities. Later, skewed-μ analysis determines maximum possible uncertainty bounds for model parameters that are difficult to identify accurately.

4.1. Uncertain quadrotor model

Stabilization of the proposed quadrotor around hover requires control of translational motion in z-axis and rotational motions similar to a standard quadrotor. Therefore, dynamical model of the vehicle is obtained which is composed of three rotational equations in roll, pitch and yaw axes, and one translational equation in z-axis. There are eight states: roll, pitch and yaw angles $\delta\eta = [\delta\phi\ \delta\theta\ \delta\psi]^T$ all in radians, body frame angular velocities $\delta\Omega = [\delta p\ \delta q\ \delta r]^T$ in radians/second, translational position and velocity in z-axis δz (in meters) and δV_z (in meters/second), respectively. Control is performed through variation in rotor speeds $\delta w = [\delta w_1\ \delta w_2\ \delta w_3\ \delta w_4]^T$ and tilt angle of small rotors $\delta\alpha_2$ and $\delta\alpha_4$. The outputs of this model are $\delta\eta$ corresponding to Euler angles in roll, pitch and yaw axes, and δz corresponding to local position in z-axis. Resulting linearized model in hover

for a rigid uncommon quadrotor is extracted from (15) as given below. Herein, $\delta\dot{\eta} = \delta\Omega$ is also satisfied.

$$\begin{bmatrix} \delta\dot{\Omega} \\ \delta\ddot{z} \end{bmatrix} = \begin{bmatrix} I^{-1} & 0 \\ 0 & m^{-1} \end{bmatrix} \begin{bmatrix} 0 & k_{f_s}l_s & 0 & -k_{f_s}l_s & k_{d_s}w_{eq2} & -k_{d_s}w_{eq4} \\ -k_{f_b}l_b & 0 & k_{f_b}l_b & 0 & k_{f_s}l_{sh}w_{eq2} & k_{f_s}l_{sh}w_{eq4} \\ k_{d_b} & k_{d_s} & -k_{d_b} & -k_{d_s} & -k_{f_s}l_s w_{eq2} & k_{f_s}l_s w_{eq4} \\ k_{f_b} & k_{f_s} & k_{f_b} & k_{f_s} & 0 & 0 \end{bmatrix} \begin{bmatrix} \delta w \\ \delta\alpha_2 \\ \delta\alpha_4 \end{bmatrix} \tag{17}$$

Therefore, nonlinear quadrotor model is approximated locally as $\bar{x} = \bar{x}_{eq} + \delta\bar{x}$, $u = u_{eq} + \delta u$ where $\delta\bar{x} = [\delta\Omega^T \ \delta\dot{z}]^T$ and $\delta u = [\delta w^T \ \delta\alpha^T]^T$.

It is assumed that parameters in this model have 10 percent uncertainty with respect to their nominal values. To give an example, $I_{xx} = \bar{I}_{xx}(1+\sigma_c\delta_1)$ where $\bar{I}_{xx}$ is a nominal value, $\sigma_c = 0.1$ is the percentage of uncertainty and $-1 < \delta_1 < 1$ is the perturbation of this parameter. Uncertain parameters are I_{xx}, I_{yy}, I_{zz}, m, k_{f_s}, l_s, w_{eq2}, w_{eq4}, k_{d_s}, k_{f_b}, l_b, l_{sh} and k_{d_b}, and they are associated with perturbations δ_1, δ_2, δ_3, δ_4, δ_5, δ_6, δ_7, δ_8, δ_9, δ_{10}, δ_{11}, δ_{12} and δ_{13}, respectively.

4.2. Finding LFT representaion

Linear fractional transformation (LFT) plays a central role in robustness analysis and robust control synthesis. Therefore, resulting closed loop should be represented with a standard $M(s)-\Delta(s)$ structure where $M(s)$ contains the dynamics of nominal model and relations of perturbations to closed loop. On the other hand, $\Delta(s)$ is constructed such that it includes all uncertainty blocks.

4.2.1. General affine state space uncertainty

In this section, it is assumed that uncertain model is represented by a state space model with unknown coefficients. Then, main aim is to compute LFT representation with respect to uncertain parameter matrix. Assume a linear system G_δ has the following state space representation, and k uncertain parameters $\delta_1, \ \delta_2, \ \ldots, \ \delta_k$ enter the state space equations in an affine way.

$$\dot{x} = (A + \sum_{i=1}^{k} \delta_i \hat{A}_i)x + (B + \sum_{i=1}^{k} \delta_i \hat{B}_i)u \quad , \quad y = (C + \sum_{i=1}^{k} \delta_i \hat{C}_i)x + (D + \sum_{i=1}^{k} \delta_i \hat{D}_i)u \tag{18}$$

In this representation, A and $\hat{A}_i \in \mathbb{R}^{n\times n}$, B and $\hat{B}_i \in \mathbb{R}^{n\times n_u}$, C and $\hat{C}_i \in \mathbb{R}^{n_y\times n}$, and D and $\hat{D}_i \in \mathbb{R}^{n_y\times n_u}$. State space equations are composed of nominal model represented with state space matrices (A, B, C, D) and effects of uncertainties determined by state space matrices (A_i, B_i, C_i, D_i) for $\delta_i \in [-1 \ \ 1]$, $i = 1, \ldots, k$. This uncertain model should be described via LFT for robustness analysis. Corresponding M_δ matrix for perturbation matrix $\Delta_p = \text{diag}(\delta_1 I, \delta_2 I, \ldots, \delta_k I)$ can be found by using the following method [18].

Obtaining LFT with the smallest possible size of repeated blocks is essential. For that reason, let q_i denote the rank of matrix $P_i := \begin{bmatrix} \hat{A}_i & \hat{B}_i \\ \hat{C}_i & \hat{D}_i \end{bmatrix} \in \mathbb{R}^{(n+n_y)\times(n+n_u)}$ for each $i = 1, \ldots, k$. Then, it is possible to write P_i as $P_i = \begin{bmatrix} L_i \\ W_i \end{bmatrix} \begin{bmatrix} R_i \\ Z_i \end{bmatrix}^*$, where $L_i \in \mathbb{R}^{n\times q_i}$, $W_i \in \mathbb{R}^{n_y\times q_i}$, $R_i \in \mathbb{R}^{n\times q_i}$ and $Z_i \in \mathbb{R}^{n_u\times q_i}$. Therefore, equation

$\delta_i P_i = \begin{bmatrix} L_i \\ W_i \end{bmatrix} \begin{bmatrix} \delta_i I_{q_i} \end{bmatrix} \begin{bmatrix} R_i \\ Z_i \end{bmatrix}^*$ is satisfied, and resulting M_δ can be found as

$$M_\delta = \underbrace{\begin{bmatrix} A & B \\ C & D \end{bmatrix}}_{M_{22}} + \underbrace{\begin{bmatrix} L_i & \dots & L_k \\ W_i & \dots & W_k \end{bmatrix}}_{M_{21}} \underbrace{\begin{bmatrix} \delta_1 I_{q_1} & & \\ & \ddots & \\ & & \delta_k I_{q_k} \end{bmatrix}}_{\Delta_p} \underbrace{\begin{bmatrix} R_1^* & Z_1^* \\ \vdots & \vdots \\ R_k^* & Z_k^* \end{bmatrix}}_{M_{12}} \tag{19}$$

which can be written as an upper LFT as $M_\delta = \mathcal{F}_u \left(\begin{bmatrix} 0 & M_{12} \\ M_{21} & M_{22} \end{bmatrix}, \Delta_p \right)$.

Resulting state space uncertainty can be represented as in Figure 2 by changing the input order of x and u to the LFT.

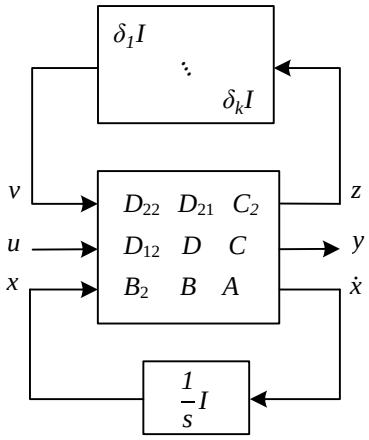

Figure 2. LFT representation of state space uncertainty

where $B_2 = \begin{bmatrix} L_1 & \dots & L_k \end{bmatrix}$, $D_{12} = \begin{bmatrix} W_1 & \dots & W_k \end{bmatrix}$, $C_2 = \begin{bmatrix} R_1 & \dots & R_k \end{bmatrix}^*$, $D_{21} = \begin{bmatrix} Z_1 & \dots & Z_k \end{bmatrix}^*$, $D_{22} = 0$ and $G_\delta(\Delta) = \mathcal{F}_l \left(\mathcal{F}_u \left(\begin{bmatrix} 0 & \bar{M}_{12} \\ \bar{M}_{21} & \bar{M}_{22} \end{bmatrix}, \Delta_p \right), \frac{1}{s} I \right)$ where $\left[\begin{array}{c|c} 0 & \bar{M}_{12} \\ \hline \bar{M}_{21} & \bar{M}_{22} \end{array}\right] = \left[\begin{array}{c|cc} D_{22} & D_{21} & C_2 \\ \hline D_{12} & D & C \\ B_2 & B & A \end{array}\right]$.

4.3. LFT representation of uncertain parameters in denominator

When an uncertain parameter is in the denominator, δ_i could not enter state space equations in an affine way. For quadrotor case, $1/I_{xx}$, $1/I_{yy}$, $1/I_{zz}$ and $1/m$ are in this form. These parameters can be represented as a LFT in δ_i as below.

$$\frac{1}{I_{xx}} = \frac{1}{\bar{I}_{xx}(1+\sigma_c\delta_1)} = \frac{1}{\bar{I}_{xx}} - \frac{\sigma_c}{\bar{I}_{xx}}\delta_1(1+\sigma_c\delta_1)^{-1} = \mathcal{F}_u \left(\begin{bmatrix} -\sigma_c & 1 \\ \frac{-\sigma_c}{\bar{I}_{xx}} & \frac{1}{\bar{I}_{xx}} \end{bmatrix}, \delta_1 \right) \tag{20}$$

Therefore, using upper LFT in (20), $\frac{1}{I_{xx}}$ can be represented where $I_{xx} = \bar{I}_{xx}(1+\sigma_c\delta_1)$. These transformations and state space uncertainty are needed to compute overall LFT of the quadrotor model.

4.4. LFT representation of proposed quadrotor model

Uncertain proposed quadrotor model can be represented as a cascade connection of two LFTs corresponding to state space uncertainty and uncertain parameters in the denominator. These systems are given below.

$$\text{System 1:} \quad \underbrace{\begin{bmatrix} \delta\ddot{\eta} \\ \delta\ddot{z} \end{bmatrix}}_{\dot{x}} = \underbrace{\begin{bmatrix} 0 & k_{f_s}l_s & 0 & -k_{f_s}l_s & k_{d_s}w_{eq2} & -k_{d_s}w_{eq4} \\ -k_{f_b}l_b & 0 & k_{f_b}l_b & 0 & k_{f_s}l_{sh}w_{eq2} & k_{f_s}l_{sh}w_{eq4} \\ k_{d_b} & k_{d_s} & -k_{d_b} & -k_{d_s} & -k_{f_s}l_s w_{eq2} & k_{f_s}l_s w_{eq4} \\ k_{f_b} & k_{f_s} & k_{f_b} & k_{f_s} & 0 & 0 \end{bmatrix}}_{B_1} \underbrace{\begin{bmatrix} \delta w \\ \delta\alpha_2 \\ \delta\alpha_4 \end{bmatrix}}_{u}, \quad y = x \tag{21}$$

$$\text{System 2:} \quad \underbrace{\begin{bmatrix} \delta\dot{\eta} \\ \delta\dot{z} \end{bmatrix}}_{\dot{x}} = \underbrace{\begin{bmatrix} I^{-1} & 0 \\ 0 & m^{-1} \end{bmatrix}}_{B_2} \underbrace{\begin{bmatrix} \delta\dot{\eta} \\ \delta\dot{z} \end{bmatrix}}_{u}, \quad y = x \tag{22}$$

Using cascade connection of LFTs, resulting LFT with respect to $\Delta_u = \text{diag}(\Delta_M, \Delta_N)$ can be obtained [19].

$$M_c = \left[\begin{array}{cc|c} M_{11} & M_{12}N_{12} & M_{12}N_{22} \\ 0 & N_{11} & N_{12} \\ \hline M_{21} & M_{22}N_{21} & M_{22}N_{22} \end{array}\right] \tag{23}$$

Here, N results from the uncertain System 1 (21), and M results from the uncertain System 2 (22). Perturbation blocks are given as $\Delta_M = \text{diag}(\delta_1, \delta_1, \delta_3, \delta_4)$ and $\Delta_N = \text{diag}(\delta_5 I_4, \delta_6 I_2, \delta_7 I_3, \delta_8 I_3, \delta_9 I_2, \delta_{10} I_2, \delta_{11}, \delta_{12}, \delta_{13})$. Resulting cascaded LFT which includes $M_c - \Delta_u$ is the overall uncertain model of the proposed quadrotor configuration. For control design purpose, system model is statically decoupled by using input decoupling (rotor mixing) matrix $T_u = \bar{B}_1^T(\bar{B}_1\bar{B}_1^T)^{-1}$. Therefore, the 4×4 model from $\delta u'$ to δy is obtained. Input decoupling matrix is fixed and calculated by using nominal values of the parameters. Therefore, for nominal case, the following transfer matrix that includes second order inertia, and mass lines are obtained.

$$P_{nominal}(s) : \delta u' \to \delta y = \text{diag}\left(\frac{1}{I_{xx}\ s^2}, \ \frac{1}{I_{yy}\ s^2}, \ \frac{1}{I_{zz}\ s^2}, \ \frac{1}{m\ s^2}\right) \tag{24}$$

This decoupled uncertain model set which is constructed by perturbing each uncertain parameter by 10 percent is visualized by following the method introduced in [20]. The first 3×3 part of the set corresponds to rotational motion, and it is shown in Figure 3. Since translational motion in z-axis and rotational motions are inherently decoupled, only 4^{th} diagonal element is given in Figure 4. Remaining elements are zero, and they are not shown. Closed loop system is constructed using manual loop shaping controller based on PI and lead filter. This controller and rotor mixing matrix T_u are depicted in Figure 5.

Remark R1: System 1 in (21) has multiplication of uncertain parameters, e.g., $k_{f_s}l_s$. These are not suitable for an affine state space uncertainty, and they should be represented with a cascade connection of LFTs corresponding to each uncertain parameter. Therefore, high order perturbations in these multiplications are neglected to obtain uncertain model easily using state space uncertainty without causing large error. Similar simplifications to $k_{f_s}l_s = \left(\bar{k}_{f_s}(1+\sigma_c\delta_5)\right)\left(\bar{l}_s(1+\sigma_c\delta_6)\right) \approx \bar{k}_{f_s}\bar{l}_s + \bar{k}_{f_s}\bar{l}_s(\sigma_c\delta_5 + \sigma_c\delta_6)$ are also used for other multiplications.

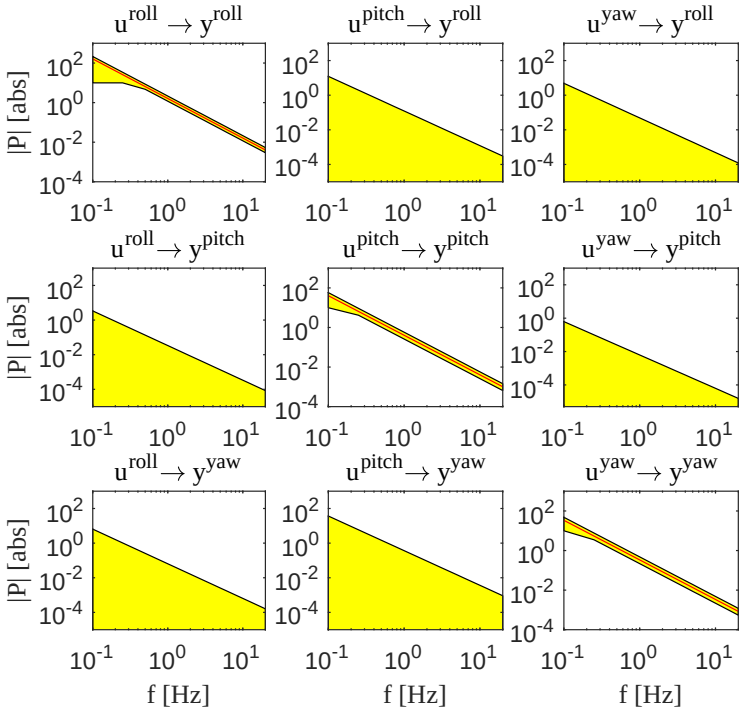

Figure 3. Rotational motion: Magnitudes of nominal model (solid red), uncertain model set (yellow shaded).

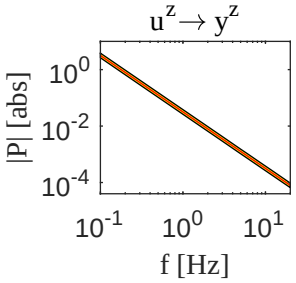

Figure 4. Translational motion in z-axis: Magnitudes of nominal model (solid red), uncertain model set (yellow shaded).

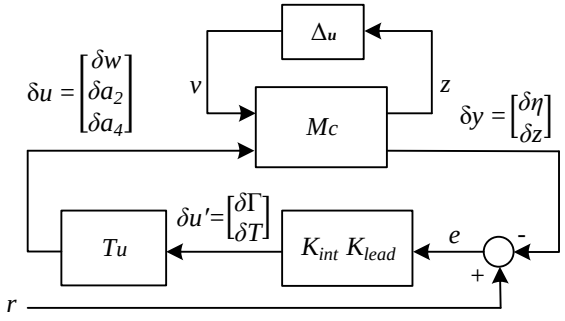

Figure 5. Feedback configuration for uncertain system.

4.5. Sensitivity analysis of the proposed quadrotor

Standard and proposed configurations both have zero state transition matrix A in the state space equations. Since A matrix is not affected from perturbed parameters, standard open loop eigenvalue sensitivity analysis fails to provide any result. Therefore, closed loop eigenvalue sensitivity analysis is more suitable for this case. Therefore, suitable controller is needed for both closed loop eigenvalue and μ sensitivity analyses.

Controller is designed using manual loop shaping principles as described in [21]. As discussed previously, axes of the plant decouple with the rotor mixing matrix. Therefore, controller for each axis can be designed separately. Following procedure can be readily applied to all axes. Firstly, suitable bandwidth which corresponds to crossover frequency f_{bw} is selected. Since each diagonal entry of the decoupled plant is of double-integrator

type, sufficient phase lead is required. This is satisfied using the following lead filter:

$$K_{lead} = p_{lead} \frac{\frac{s}{2\pi \frac{1}{3} f_{bw}} + 1}{\frac{s}{2\pi 3 f_{bw}} + 1} \ . \tag{25}$$

p_{lead} is adjusted to satisfy $|GK_{lead}(2\pi f_{bw})|$=1. With the lead filter, compensated loop satisfies -1 slope in the crossover region which is essential for sufficient robustness. Next, for command tracking and disturbance rejection, PI controller is added with integral cut-off at $f_{bw}/5$ to keep the phase margin unaffected due to zero at $f_{bw}/5$, i.e., $K_{int} = \frac{s+2\pi \frac{f_{bw}}{5}}{s}$. $K = K_{int}K_{lead}$ is the resulting controller for one axis. In this way, 42° phase margin and infinite gain margin are achieved in each channel for nominal model. Selected f_{bw} is 2 Hz for roll and pitch axes of rotational motion. For yaw axis, f_{bw} is selected as 0.4 Hz. For translational motion in z-axis, 0.25 Hz is aimed. Authors obtained similar bandwidths for multirotors in couple of experimental studies. Since similar values are often achieved in practice, these bandwidths are selected. Overall diagonal (decentralized) multiple input multiple output (MIMO) controller is obtained by putting single input single output (SISO) controllers at the diagonal entries according to axis order. This controller is used during closed loop sensitivity analysis. In this analysis, parameters of the proposed quadrotor given in Table 1 are used.

Table 1. Physical parameters of the proposed quadrotor configuration

Total weight of the vehicle	m	0.8 kg
Gravitational acceleration	g	9.81 m/s^2
Moment of inertia along x-axis	I_{xx}	15.67×10^{-3} kgm^2
Moment of inertia along y-axis	I_{yy}	62.68×10^{-3} kgm^2
Moment of inertia along z-axis	I_{zz}	75.20×10^{-3} kgm^2
Big arm length of the quadrotor	l_b	0.6 m
Small arm length of the quadrotor	l_s	0.3 m
Thrust factor of big rotor	k_{f_b}	769.28×10^{-7} $N/(rad/s)^2$
Thrust factor of small rotor	k_{f_s}	192.32×10^{-7} $N/(rad/s)^2$
Drag factor of big rotor	k_{d_b}	16.012×10^{-7} $Nm/(rad/s)^2$
Drag factor of small rotor	k_{d_s}	4.003×10^{-7} $Nm/(rad/s)^2$
Square of small rotor speed in hover	w_{eq2}, w_{eq4}	$(110)^2$ $(rad/s)^2$
Distance from the mass center to small rotor along z-axis	l_{sh}	0.03 m

Closed loop eigenvalue sensitivity is performed using average of the eigenvalue sensitivities (26) for each parameter where the sensitivity of the i^{th} eigenvalue λ_i, $i = 1, \ldots, 16$ to variations in the j^{th} parameter p_j, $j = 1, \ldots, 13$ is defined as (27).

$$Sen^{\lambda}_{p_j} = \frac{1}{16} \sum_{i=1}^{16} Sen^{\lambda_i}_{p_j} \tag{26}$$

$$Sen^{\lambda_i}_{p_j} = \frac{\partial \lambda_i(p)}{\partial p_j} \approx \frac{|\lambda_i(p + \Delta p_j) - \lambda_i(p)|}{\Delta p_j} \tag{27}$$

16 closed loop eigenvalues result from combination of 8 plant and 8 controller eigenvalues. Figure 6 shows the eigenvalue sensitivities for each uncertain parameter when $\delta_j = 1$ which corresponds to 10 percent perturbation

in each uncertain parameter. It shows that uncertain parameters k_{f_s}, l_s, w_{eq2}, w_{eq4} and l_{sh} (i.e., δ_5, δ_6, δ_7, δ_8 and δ_{12}) have correspondingly large effects on closed loop eigenvalues. In addition, I_{xx} and I_{yy} (i.e., δ_1 and δ_2) have equal effects on closed loop since controller is designed to obtain equal closed loop performance in roll and pitch axes. On the other hand, effects of I_{zz}, m, k_{d_s}, k_{f_b}, l_b and k_{d_b} (i.e., δ_3, δ_4, δ_9, δ_{10}, δ_{11} and δ_{13}) to this closed loop are small. Different controller selection may change the sensitivities; however, the relative importances of the parameters remain the same if similar control performances are aimed for all axes.

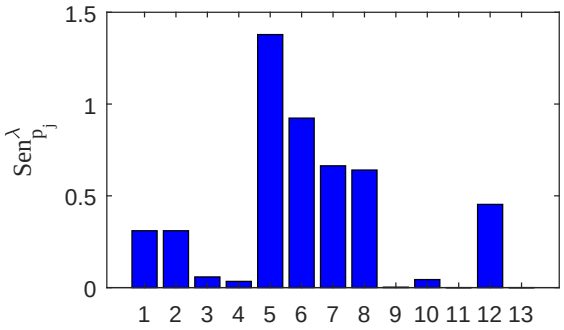

Figure 6. Closed loop eigenvalue sensitivity analysis.

The aim of the sensitivity analysis is to measure a change in a system behavior due to parameter perturbations. In eigenvalue sensitivity analysis, a system behavior is determined by a change in eigenvalues. If a system behavior is determined by a structured singular value μ, relative importance of uncertain parameters on system robustness can be found using μ sensitivities. Robust performance and robust stability can be selected for μ sensitivity analysis. Let $M = \begin{bmatrix} M_{11} & M_{12} \\ M_{21} & M_{22} \end{bmatrix}$ be internally stable. Then, robust stability (RS) test is $\mu_{\Delta}(M_{11}) < 1,\ \forall w$, and robust performance (RP) test is $\mu_{\bar{\Delta}}(M) < 1,\ \forall w$ where $\bar{\Delta} = \mathrm{diag}(\Delta, \Delta_p)$, and Δ_p is a fictitious uncertainty block representing the $\mathcal{H}_\infty$ performance specification [18].

$$Sen^{\mu}_{p_j} = \frac{\partial \mu(M)}{\partial p_j} \approx \frac{\mu(M_\epsilon) - \mu(M)}{\Delta p_j} \tag{28}$$

For RP, μ sensitivity of the j^{th} parameter p_j is defined as (28) where M_ϵ denotes a perturbed system, and Δp_j denotes a percentage change of an associated normalized parameter. For that, each $\delta_i I_i$ is multiplied by a_i, where each a_i is real and nominally one except for the j^{th} perturbed scalar $a_j = 1 + \epsilon$. Therefore, matrix $a = \mathrm{diag}(I_1,\ I_2,\ \ldots,\ a_j I_j,\ \ldots,\ I_{k-1},\ I_k)$ is useful. Instead of using $a\Delta$ for original M, a can be absorbed into M, and perturbed system M_ϵ is obtained for original Δ as $M_\epsilon = \begin{bmatrix} aM_{11} & aM_{12} \\ M_{21} & M_{22} \end{bmatrix}$.

Positive ϵ corresponds to non-decreasing function $\mu(M_\epsilon)$ which implies that μ sensitivities are always non-negative. Similarly, for RS, μ sensitivity of the j^{th} parameter p_j is defined as

$$Sen^{\mu}_{p_j} = \frac{\partial \mu(M_{11})}{\partial p_j} \approx \frac{\mu(aM_{11}) - \mu(M_{11})}{\Delta p_j}\ . \tag{29}$$

In this article, variations of the parameters to robust stability is investigated, and the definition (29) is used.

Remark R2: In practice, μ lower or upper bound is used instead of μ since exact calculation of μ is NP-hard [16]. Upper bound gives (possibly conservative) maximum allowable size of uncertainty to satisfy robustness requirements, whereas lower bound gives the smallest uncertainty which violates robustness requirements. During μ sensitivity analysis, upper bound is used since the computation of upper bound is convex, i.e., only minimum is global. Using μ upper bound can give different values from exact sensitivity values; however, the relative importances of the uncertain parameters on robust stability or performance are not affected [16].

μ sensitivities are calculated by using a mixed upper-bound μ algorithm [22] and perturbing each normalized parameter with $\delta_i = 0.5$. This corresponds to 5 percent deviation from the nominal value since each normalized parameter has 10 percent uncertainty. Figure 7 shows the μ sensitivities for each uncertain parameter. Uncertain parameters k_{f_s}, l_s, w_{eq2}, w_{eq4}, k_{d_s} and l_{sh} (i.e., δ_5, δ_6, δ_7, δ_8, δ_9 and δ_{12}) are more important in terms of robust stability. These parameters were also important in terms of closed loop eigenvalues except k_{d_s} and l_{sh} which were less important for closed loop eigenvalue sensitivity. Importance of the remaining parameters on robust stability and closed loop eigenvalue sensitivity differs. Therefore, traditional eigenvalue sensitivity analysis may fail to find critical parameters in terms of closed loop stability. In the next section, allowable level of uncertainty for each parameter will be investigated.

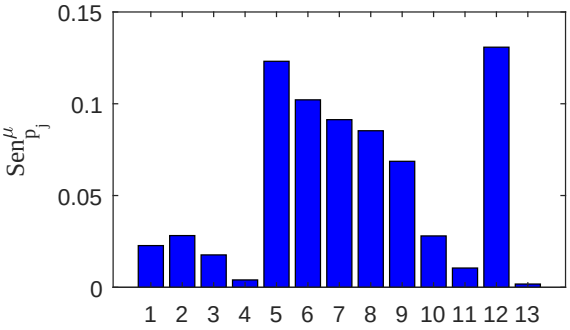

Figure 7. μ sensitivity analysis.

4.6. Control oriented uncertainty modeling

Skewed structured singular value, $\mu_{s,\bar{\Delta}}$, of a matrix M with respect to uncertain matrix $\bar{\Delta} = \mathrm{diag}(\Delta_v,\ \Delta_f)$ is defined as $\mu_{s,\bar{\Delta}} = \left(\min\{\bar{\sigma}(\Delta_v) \mid\ \bar{\sigma}(\Delta_f) \leq 1,\ \det(I - M\bar{\Delta}) = 0\}\right)^{-1}$. Skewed structured singular value is valuable if some partitions of the uncertainty block are already known, and minimization is performed over the unknown parts. In this section, $\mu_{s,\bar{\Delta}}$ is used to find maximum allowable size of uncertainty block Δ_v without violating robust stability when the remaining part $\bar{\sigma}(\Delta_f) \leq 1$, i.e., parameters in this portion are allowed to vary in $\sigma_c = 0.1 = 10\%$. In this way, maximum possible perturbations of the parameters which are difficult or costly to estimate can be found, while remaining parameters are within 10% bound.

In the dynamic model, thrust constants k_{f_s} and k_{f_b}, rotor drag constants k_{d_s} and k_{d_b} and square of small rotor speeds in hover w_{eq2} and w_{eq4} are most difficult and costly to estimate. In addition, variations of these parameters are large since they are affected from environmental conditions and battery voltage. Therefore, maximum allowable perturbations for k_{f_s}, w_{eq2}, w_{eq4}, k_{d_s}, k_{f_b} and k_{d_b} (i.e., δ_5, δ_7, δ_8, δ_9, δ_{10} and δ_{13}) are investigated, while remaining parameters are kept within 10% bound. Similarly, maximum allowable

perturbations for k_{f_s}, k_{f_b}, k_{d_s} and k_{d_b} (i.e., δ_5, δ_9, δ_{10} and δ_{13}) are also analyzed by assuming that w_{eq2} and w_{eq4} can be estimated online during hovering. Initial uncertainty bounds for all normalized parameters are 10% corresponding to $\sigma_c = 0.1$. During this analysis, mixed lower-bound skewed-μ algorithm is used [22].

Six models are selected such that Δ_f and Δ_v are constructed with different combinations of uncertain parameters. In model 1, all uncertain parameters are in Δ_v, which turns skewed-μ into standard μ lower bound computation. Model 2 to 5 are constructed by increasing the number of parameters, which are easy to estimate or measure in Δ_f. In model 6, w_{eq2} and w_{eq4} (i.e., δ_7 and δ_8) are also placed in Δ_f. These six models are illustrated in Table 2.

Worst case parameter combinations for all six models are given in Table 3. Relative uncertainty bounds between different uncertain parameters are illustrated. Values given in bold correspond to six parameters which are the most difficult to identify.

Table 2. Models for skewed-μ analysis.

Model	Δ_f	Δ_v
1	$\{-\}$	$\{\delta_1, \delta_2, \delta_3, \delta_4, \delta_5, \delta_6, \delta_7, \delta_8, \delta_9, \delta_{10}, \delta_{11}, \delta_{12}, \delta_{13}\}$
2	$\{\delta_1, \delta_3\}$	$\{\delta_2, \delta_4, \delta_5, \delta_6, \delta_7, \delta_8, \delta_9, \delta_{10}, \delta_{11}, \delta_{12}, \delta_{13}\}$
3	$\{\delta_1, \delta_2, \delta_3, \delta_4\}$	$\{\delta_5, \delta_6, \delta_7, \delta_8, \delta_9, \delta_{10}, \delta_{11}, \delta_{12}, \delta_{13}\}$
4	$\{\delta_1, \delta_2, \delta_3, \delta_4, \delta_6, \delta_{11}\}$	$\{\delta_5, \delta_7, \delta_8, \delta_9, \delta_{10}, \delta_{12}, \delta_{13}\}$
5	$\{\delta_1, \delta_2, \delta_3, \delta_4, \delta_6, \delta_{11}, \delta_{12}\}$	$\{\delta_5, \delta_7, \delta_8, \delta_9, \delta_{10}, \delta_{13}\}$
6	$\{\delta_1, \delta_2, \delta_3, \delta_4, \delta_6, \delta_7, \delta_8, \delta_{11}, \delta_{12}\}$	$\{\delta_5, \delta_9, \delta_{10}, \delta_{13}\}$

Table 3. Worst-case parameter combinations for skewed-μ analysis models.

Model	δ_1	δ_2	δ_3	δ_4	δ_5	δ_6	δ_7	δ_8	δ_9	δ_{10}	δ_{11}	δ_{12}	δ_{13}
1	-2.77	-2.89	2.74	0.07	**-2.90**	-2.90	**2.90**	**-2.90**	**2.90**	**2.90**	2.90	-2.90	**-2.83**
2	-1.00	2.90	-1.00	0.001	**-2.90**	-2.90	**2.90**	**-2.90**	**2.90**	**2.90**	2.90	-2.90	**-2.85**
3	-1.00	1.00	-1.00	0.001	**-2.90**	-2.90	**2.90**	**-2.90**	**2.90**	**2.90**	2.90	-2.90	**-2.85**
4	0.17	-0.73	0.43	0.18	**-3.33**	-0.79	**-3.33**	**-3.33**	**2.64**	**-3.33**	-1.00	-3.33	**3.33**
5	0.23	0.95	-0.99	0.001	**-3.93**	-1.00	**3.93**	**-3.93**	**3.93**	**3.93**	1.00	-1.00	**-2.62**
6	0.02	0.99	-0.99	0.001	**-6.14**	-1.00	**1.00**	**-1.00**	**6.14**	**6.14**	1.00	-1.00	**-6.14**

It is observed that model 1, 2 and 3 result in a similar destabilizing perturbation norm. For example, when δ_1, δ_2, δ_3 and δ_4 are in Δ_f, worst case perturbation occurs at $\bar{\sigma}_c = 2.90$. This corresponds to allowable 29% uncertainty ($\bar{\sigma}_c \sigma_c = 0.29$) for δ_5, δ_6, δ_7, δ_8, δ_9, δ_{10}, δ_{11}, δ_{12} and 28.5% uncertainty for δ_{13} for robust stability. In model 3, I_{xx}, I_{yy} and I_{zz} have 10% percent allowable uncertainty. However, worst case performance occurs when $\delta_4 = 0.001$. This illustrates that 0.01% uncertainty in m is tolerable. As given in model (17), remaining uncertain parameters in Δ_v are divided by I_{xx}, I_{yy}, I_{zz} and m. Therefore, allowable perturbations for I_{xx}, I_{yy}, I_{zz} and m tend to be smaller when allowable perturbations in the remaining parameters increase. Table 3 shows that worst case perturbations occur when some of the allowable uncertainties are small for I_{xx}, I_{yy}, I_{zz} and m which are in the denominator. On the contrary, norms of the remaining parameters in the numerator are maximized. Therefore, to tolerate large uncertainties in the remaining parameters, these physical parameters should be measured accurately. When δ_6 and δ_{11} are added to Δ_f in model 4, tolerable uncertainty rises to

3.33. In other words, 33.3% uncertainty is allowed for k_{f_s}, w_{eq2}, w_{eq4}, k_{f_b}, l_{sh}, k_{d_b} and 26.4% for k_{d_s}. For this case, I_{xx}, I_{yy}, I_{zz}, m, l_s and l_b are need to known with 1.7%, 7.3%, 4.3%, 1.8%, 7.9% and 10% error, respectively. In model 5, l_{sh} is added to Δ_f part, and allowed perturbation in the remaining parameters rises to 39.3% except k_{d_b} which is limited to 26.2%. In model 6, 61.4% uncertainty in k_{f_s}, k_{f_b}, k_{d_s} and k_{d_b} is tolerable if I_{xx}, I_{yy}, I_{zz}, m, l_s, w_{eq2}, w_{eq4}, l_b and l_{sh} are known with 0.2%, 9.9%, 9.9%, 0.01%, 10%, 10%, 10%, 10% and 10% error, respectively. Therefore, by reducing the uncertainties in easily measurable parameters, large variations in the remaining uncertain parameters which are difficult or expensive to identify are allowed.

5. Comments

As shown in Figure 3, parameter perturbations induce significant dynamics at the off-diagonal elements of statically decoupled plant model with constant matrix T_u. Worst case perturbations usually occur when these coupling dynamics destabilize the corresponding axis. If larger variations in the parameters are desired, coupling effects due to perturbations should be analyzed carefully. In addition, finding easily measurable parameters with very small uncertainty allows larger variations in the remaining parameters. In this way, effort and budget required to obtain parameters that are difficult to estimate can be reduced.

6. Conclusion

UAVs have gained popularity in the last two decades. Among all, quadrotors have been used in various military and civil applications. However, typical quadrotor has limited flight endurance due to high energy consumption. Therefore, alternative configurations have been investigated to increase the efficiency and, hence, flight endurance compared to a standard quadrotor. In this article, an uncommon quadrotor configuration is proposed for that purpose.

Since this configuration is not common, flight control requires dynamical model of this vehicle. In this study, aim is to use this vehicle at slow velocities around hover position. Therefore, a linear model can resemble the actual dynamics sufficiently around hover position. For that, linear model is obtained and pseudoinverse based input decoupling (rotor mixing) matrix is introduced.

Model based on physical principles are frequently used in flight control designs. In this case, bounds on model parameters are widely used, and control designs should give sufficient performance under these parameter variations. But, required performance may not be achieved with fixed controller if variations in these parameters are large. In that case, some parameters should be determined more accurately. Therefore, understanding which parameters mostly disturb the robust stability or performance is essential. Structured singular value sensitivity analysis is introduced for that purpose. In addition, some of the parameters in the model are much more difficult to estimate. Maximum allowable uncertainty in these parameters for closed loop stability can also be calculated. This is mostly valuable in aerospace control applications where there are large uncertainties in the parameters, and identification tests are difficult and expensive. Next, parameters of the uncommon quadrotor model are analyzed, and important ones in terms of robust stability are found. It is observed that when easily determined parameters are known more accurately, allowable uncertainties increase for the remaining parameters that are difficult to estimate.

In this article, an uncommon quadrotor configuration is proposed to increase the efficiency and hence flight endurance. But some parts require further attention. Firstly, efficiency of this vehicle should be calculated theoretically and compared with the standard case. Secondly, a prototype of this configuration should be

constructed. Later, results of this study should be verified with experimental measurements. Next, dynamics of rotor speed and tilt angle control should be included in the system model. Finally, aerodynamic effects and larger deviations from hover position should also be considered.

References

[1] Mahony R, Kumar V, Corke P. Multirotor aerial vehicles: Modeling, estimation, and control of quadrotor. IEEE Robotics and Automation magazine 2012; 19 (3): 20-32. doi:10.1109/MRA.2012.2206474

[2] Sani MF, Shoaran M, Karimian G. Automatic landing of a low-cost quadrotor using monocular vision and Kalman filter in GPS-denied environment. Turkish Journal of Electrical Engineering & Computer Sciences 2019; 27 (3): 1821-1838. doi:10.3906/elk-1809-204

[3] Mulgaonkar Y, Whitzer M, Morgan B, Kroninger CM, Harrington A et al. Power and weight considerations in small, agile quadrotors. In: SPIE Defense + Security; Maryland, USA; 2014.

[4] Driessens S, Pounds P. The triangular quadrotor: a more efficient quadrotor configuration. IEEE Transactions on Robotics 2015; 31 (6): 1517-1526. doi:10.1109/TRO.2015.2479877

[5] Hoffmann GM, Huang H, Waslander SL, Tomlin CJ. Quadrotor helicopter flight dynamics and control: Theory and experiment. In: AIAA guidance, navigation and control conference and exhibit; South Carolina, USA; 2007.

[6] Kim T, Hong S. Control system design and experimental validation of hybrid multicopter for endurance enhancement. Asia-pacific Journal of Modeling and Simulation for Mechanical System Design and Analysis (AJMSM) 2017; 2 (1) 15-20. doi:10.21742/ajmsm.2017.2.1.03

[7] Pang T, Peng K, Lin F, Chen BM. Towards long-endurance flight: Design and implementation of a variable-pitch gasoline-engine quadrotor. In: IEEE International Conference on Control and Automation (ICCA); Nepal; 2016.

[8] Haus T, Orsag M, Bogdan S. Design considerations for a large quadrotor with moving mass control. In: International Conference on Unmanned Aircraft Systems (ICUAS); Arlington, USA; 2016.

[9] Yeair [online]. Website https://yeair.de/ [accessed 14 05 2021].

[10] Raffo GV, Ortega MG, Rubio FR. An integral predictive/nonlinear H_∞ control structure for a quadrotor helicopter. Automatica 2010; 46 (1): 29-39. doi:10.1016/j.automatica.2009.10.018

[11] Doukhi O, Fayjie AR, Lee DJ. Intelligent controller design for quad-rotor stabilization in presence of parameter variations. Journal of Advanced Transportation 2017. doi:10.1155/2017/4683912

[12] Labbadi M, Cherkaoui M. Robust adaptive backstepping fast terminal sliding mode controller for uncertain quadrotor UAV. Aerospace Science and Technology 2019; 93. doi:10.1016/j.ast.2019.105306

[13] Qin Y, Xu W, Lee A, Zhang F. Gemini: A compact yet efficient bi-copter uav for indoor applications. IEEE Robotics and Automation Letters 2020; 5 (2): 3213-3220. doi:10.1109/LRA.2020.2974718

[14] Baskın M, Leblebicioğlu K. Combined system identification and robust control of a gimbal platform. Turkish Journal of Electrical Engineering & Computer Sciences 2021; 29 (4): 2247-2262. doi:10.3906/elk-2009-74

[15] Baskın M, Leblebicioğlu K. Robust control for line-of-sight stabilization of a two-axis gimbal system. Turkish Journal of Electrical Engineering & Computer Sciences 2017; 25 (5): 3839-3853. doi:10.3906/elk-1606-435

[16] Marcos A, Bates D, Postlethwaite I. Control oriented uncertainty modelling using μ sensitivities and skewed μ analysis tools. In: IEEE Conference on Decision and Control; Seville, Spain; 2005.

[17] Hespanha JP. Linear systems theory. New Jersey, USA: Princeton university press, 2009.

[18] Zhou K, Doyle JC, Glover K. Robust and optimal control. New Jersey, USA: Prentice hall, 1996.

[19] Lambrechts P, Terlouw J, Bennani S, Steinbuch M. Parametric uncertainty modeling using LFTs. In: American Control Conference; California, USA; 1993.

[20] Oomen T, Quist S, van Herpen R, Bosgra O. Identification and visualization of robust-control-relevant model sets with application to an industrial wafer stage. In: IEEE Conference on Decision and Control; USA; 2010.

[21] Oomen T, Steinbuch M. Model-based control for high-tech mechatronic systems. CRC Press, 2020.

[22] Roos C. Systems modeling, analysis and control (SMAC) toolbox: An insight into the robustness analysis library. In: IEEE Conference on Computer Aided Control System Design (CACSD); Hyderabad, India; 2013.